*IRWIN AND JOAN JACOBS*
*CENTER FOR COMMUNICATION AND INFORMATION TECHNOLOGIES*

# Multi scatter, Multi view Monte Carlo radiative transfer

**Vadim Holodovsky,**
**Yoav Y. Schechner, Anat Levin,**
**Aviad Levis, Amit Aides**

**CCIT Report #889**
**November 2015**


*DEPARTMENT OF ELECTRICAL ENGINEERING*
*TECHNION - ISRAEL INSTITUTE OF TECHNOLOGY, HAIFA 32000, ISRAEL*

CCIT Report #889 November 2015

# Multi scatter, Multi view Monte Carlo radiative transfer

Vadim Holodovsky,[1*] Yoav Y. Schechner,[1] Anat Levin,[2]
Aviad Levis,[1] Amit Aides,[1]

[1]Dept of Electrical Engineering,
Technion - Israel Institute of Technology,
Haifa 32000, Israel

[2]Dept of Mathematics and Computer Science,
Weizmann - Institute of Science,
Rehovot, 76100 Israel
{vholod@tx.technion.ac.il}

november 10, 2015

## 1 Theoretical background

**Extinction**: Radiance is a flow of photons. Light propagation through the atmosphere is affected by interaction with air molecules and aerosols (airborne particles). Atmospheric constituents have an *extinction cross section* for interaction with each individual photon. Per unit volume, the *extinction coefficient* due to aerosols is $\beta^{\text{aerosol}} = \sigma^{\text{aerosol}} n$. Here $\sigma^{\text{aerosol}}$ denotes aerosol extinction cross section and $n$ denotes particle density. The total extinction is a sum of the aerosol and molecular contributions, $\beta = \beta^{\text{aerosol}} + \beta^{\text{air}}$, where $\beta^{\text{air}}$ is modeled as a function of altitude and wavelength $\lambda$ [5]. The *optical depth* along a photon path $S$ is

$$\tau = \int_S d\tau = \int_S (\beta^{\text{aerosol}} + \beta^{\text{air}}) dl = \int_S (\sigma^{\text{aerosol}} n + \beta^{\text{air}}) dl = \tau^{\text{air}} + \int_S \sigma^{\text{aerosol}} n dl \ , \tag{1}$$

where $\tau^{\text{air}} = \int \beta^{\text{air}} dl$. Through a non-scattering atmosphere, the *transmittance* exponentially decays with the optical depth:

$$t = \exp(-\tau) \ . \tag{2}$$

**Scattering**: Suppose that a photon interacts with a single particle. The unitless *single scattering albedo* $\varpi$ of the particle, determines a probability for scattering. The aerosol single scattering albedo is $\varpi^{\text{aerosol}}$. The *scattering coefficient* due to aerosols in the volume is $\alpha^{\text{aerosol}} = \varpi^{\text{aerosol}} \beta^{\text{aerosol}} = \varpi^{\text{aerosol}} \sigma^{\text{aerosol}} n$. For non-isotropic scattering, an angular function defines the probability of photons to scatter into each direction. Let $\boldsymbol{\omega}, \boldsymbol{\psi} \in \mathbb{S}^2$ (unit sphere) represent photon or ray directions. The fraction of energy scattered from direction $\boldsymbol{\psi}$ towards direction $\boldsymbol{\omega}$ is determined by a *phase function* $P(\boldsymbol{\omega} \cdot \boldsymbol{\psi})$. The phase function is normalized: its integral over all solid angles is unity, and is often approximated by a parametric expression. Specifically, the Henyey-Greenstein function, parameterized by an *anisotropy parameter* $-1 \geq g \geq 1$, can approximate aerosol scattering [5]

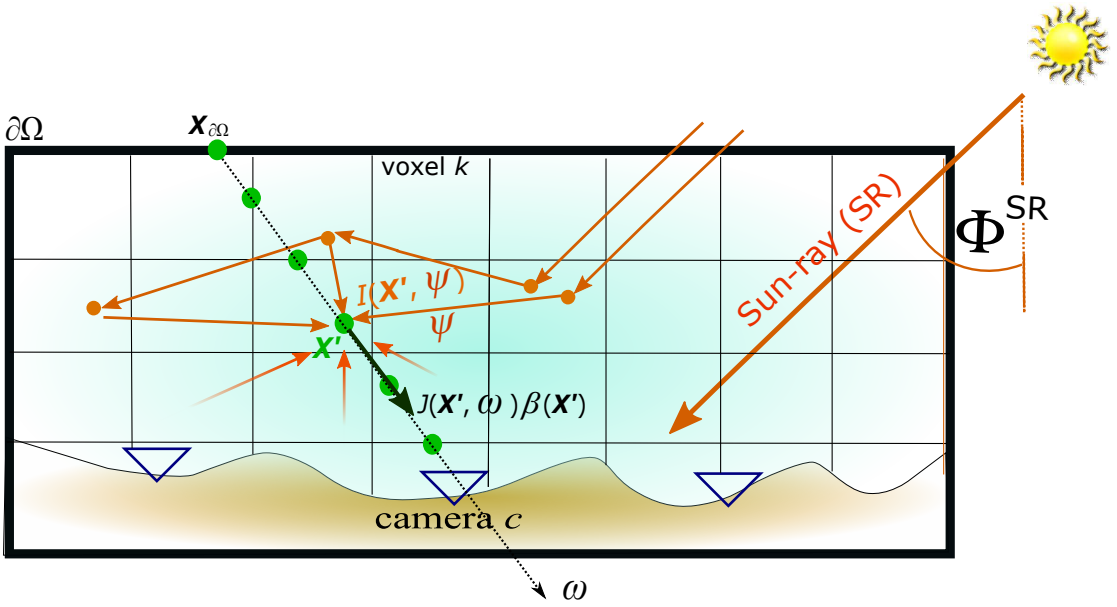


Figure 1: Integral (lightfield) imaging through a volumetric distribution in the atmosphere, using ground-based cameras.

$$P_{\mathrm{HG}}(\boldsymbol{\omega}\cdot\boldsymbol{\psi}) = \frac{1}{4\pi}\frac{1-g^2}{\left[1+g^2-2g(\boldsymbol{\omega}\cdot\boldsymbol{\psi})\right]^{\frac{3}{2}}}. \tag{3}$$

Scattering by air molecules follows the *Rayleigh* model

$$P_{\mathrm{Ray}}(\boldsymbol{\omega}\cdot\boldsymbol{\psi}) = \frac{3}{16\pi}\left[1+(\boldsymbol{\omega}\cdot\boldsymbol{\psi})^2\right]. \tag{4}$$

In the visible range, air single scattering albedo is $\varpi^{\mathrm{air}} \simeq 1$ and emission is negligible. For simplicity, wavelength dependency is omitted.

**Radiative Transfer Equation**: The radiative transfer equation (RTE) describes the flow of radiance $I(\mathbf{X}, \boldsymbol{\omega})$ at position $\mathbf{X}$, through a scattering medium [13]

$$\nabla_{\boldsymbol{\omega}} I(\mathbf{X}, \boldsymbol{\omega}) = -\beta(\mathbf{X}) I(\mathbf{X}, \boldsymbol{\omega}) + \beta(\mathbf{X}) J(\mathbf{X}, \boldsymbol{\omega}). \tag{5}$$

Here $J(\mathbf{X}, \boldsymbol{\omega})$ is the *in scattering* [13] volumetric field

$$J(\mathbf{X}, \boldsymbol{\omega}) = \varpi \int_{4\pi} P(\boldsymbol{\omega}, \boldsymbol{\psi}) I(\mathbf{X}, \boldsymbol{\psi}) d\boldsymbol{\psi}. \tag{6}$$

Denote the medium boundary by $\partial\Omega$ and the boundary radiance as $I_{\partial\Omega}$. Let $\mathbf{X}_{\partial\Omega}$ be the intersection point of the boundary with a ray in direction $\boldsymbol{\omega}$. Integrating Eq. (5) along direction $\boldsymbol{\omega}$ defines the

integral form of the RTE (Fig. 1)

$$I(\mathbf{X},\boldsymbol{\omega}) = I_{\partial\Omega}\exp\Big[-\int_{\mathbf{X}}^{\mathbf{X}_{\partial\Omega}}\beta(r)dr\Big] + \int_{\mathbf{X}}^{\mathbf{X}_{\partial\Omega}} J(\mathbf{X}',\boldsymbol{\omega})\beta(\mathbf{X}')\exp\Big[-\int_{\mathbf{X}}^{\mathbf{X}'}\beta(r)dr\Big]d\mathbf{X}'. \tag{7}$$

Monte Carlo (MC) is a popular numerical approach to solve Eqs. (5,6,7).

## 1.1 Monte Carlo Photon Tracking

Monte-Carlo is a stochastic approach that treats scattering and extinction as random phenomena sampled from probability distributions. An inverse transform [6] samples random events according to a specified probability density function. Let $u$ be a random number drawn from a uniform distribution in the unit interval: $u \sim \mathscr{U}[0,1]$. The number $u$ can be transformed into a random variable $\chi$, whose cumulative distribution function (CDF) is $F(\chi)$. The transform is defined by $\chi = F^{-1}(u)$, where $F^{-1}$ denotes the inverse of $F$. For example consider a photon propagating in the atmosphere. The photon has high probability of propagating as long as $t$ is high, but the probability diminishes as $t \to 0$. Thus Eq. (2) can be viewed as a probability density function, whose CDF is

$$F(\tau) = \int_0^{\tau} \exp(-\tau')\,d\tau' = 1 - \exp(-\tau). \tag{8}$$

Each photon then propagates to a random optical depth

$$\tau^{\text{random}} = F^{-1}(u) = -\ln(1-u). \tag{9}$$

Let location $\mathbf{X}_c$ to be the center of projection of a modeled camera $c$. Each pixel $p$ collects radiation flowing from a narrow cone around direction $\boldsymbol{\omega}_p$. The raw image is $i_c(\boldsymbol{\omega}_p)$. In order to derive images $i_c(\boldsymbol{\omega}_p)$, we describe two existing MC approaches [10].

1. Forward Monte Carlo (FMC): photons propagate from the source (sun) to the detector.
2. Backward Monte Carlo (BMC): photons propagate from the detector to the source.

### 1.1.1 Forward Monte Carlo Photon Tracking

In this approach, photons are generated at the source, illuminating the top of the atmosphere (TOA) uniformly. Photons propagate from the TOA in direction $\boldsymbol{\omega}_{\text{sun}}$. Each photon is traced through the atmosphere. Photons that happen to reach camera $c$ about direction $\boldsymbol{\omega}_p$ are counted as a contribution to $i_c(\boldsymbol{\omega}_p)$. A photon's life cycle is then defined by the following steps (Fig. 2):

(`i`) Launch a photon-packet from the TOA in direction $\boldsymbol{\omega}_{\text{sun}}$. This is the initial *ray*, denoted $\mathscr{R}_0$. The packet has initial intensity $I_0$.

Per iteration $s$:

(`ii`) Find the distance on ray $\mathscr{R}_s$ to which the photon-packet propagates. Eq. (9) yields $\tau^{\text{random}}$. Then using Eq. (1), numerically seek $l^{\text{random}}$ s.t.

$$\int_0^{l^{\text{random}}} (\sigma^{\text{aerosol}} n + \beta^{\text{air}})dl = \tau^{\text{random}}. \tag{10}$$

Distance $l^{\text{random}}$ along $\mathscr{R}_s$ yields the 3D position $\mathbf{X}_s$.

(`iii`) If $\mathbf{X}_s$ is outside the domain, the packet is terminated. If $\mathscr{R}_s$ passes through $\mathbf{X}_c$, or a small area around $\mathbf{X}_c$, the packet is counted as contributing to the image pixel.

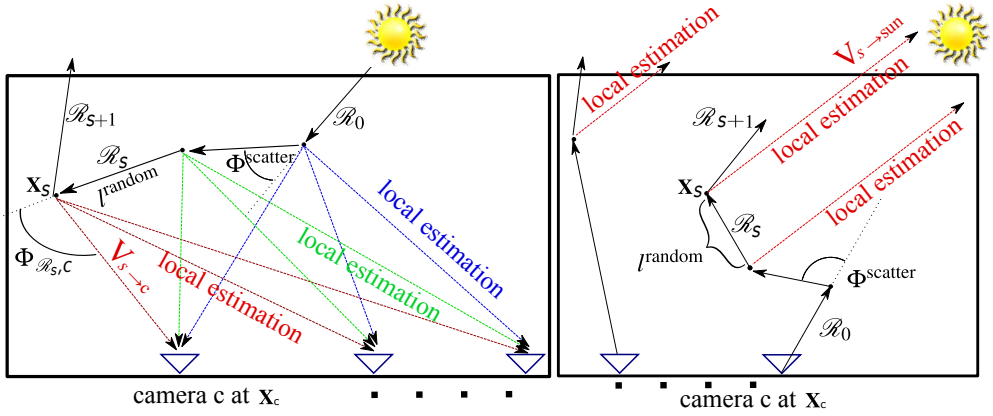


Figure 2: [Left] Multi-view FMC with local estimation. [Right] Multi-view BMC with local estimation..

(iv) The type of particle (air molecule or aerosol) that the photon-packet interacts with at point $\mathbf{X}_s$ is randomly determined by the relative extinction coefficients ($\beta^{\text{air}}$ vs. $\beta^{\text{aerosol}}$) at the voxel containing $\mathbf{X}_s$.

(v) If the particle is an aerosol, the photon-packet intensity is attenuated to $I_{s+1} = \varpi^{\text{aerosol}} I_s$. If $I_{s+1}$ is lower than a threshold, the packet is stochastically terminated, following [3].

(vi) The photon-packet is scattered to a new random direction, determined by inverse transform sampling [14,15], according to the phase function of the particle (Eqs. 3,4). Let $\Phi^{\text{scatter}} = \arccos(\boldsymbol{\omega} \cdot \boldsymbol{\psi})$ be the off-axis scattering angle, relative to $\boldsymbol{\psi}$. Given a random sample $u \sim \mathscr{U}[0,1]$,

$$\Phi^{\text{scatter}} = \arccos\left\{ \frac{1}{2g}\left[1 + g^2 - \left(\frac{g^2 - 1}{1 + 2gu - g}\right)\right]\right\} \tag{11}$$

for an aerosol particles, and

$$\Phi^{\text{scatter}} = \arccos(\gamma^{\frac{1}{3}} - \gamma^{-\frac{1}{3}}) \qquad \text{with} \qquad \gamma = 4u - 2 + \left[(4u-2)^2 + 1\right]^{\frac{1}{2}} \tag{12}$$

for molecules. The scattering azimuth angle around $\boldsymbol{\psi}$ is sampled from $\mathscr{U}[0, 2\pi]$. Following this scattering event, the photon traces a new *ray*, denoted $\mathscr{R}_{s+1}$, and the next iteration of propagation (ii) proceeds.

### 1.1.2 Local Estimation In FMC

The quality of FMC increases with the number of photons launched. Photons contributing to any pixel are accumulated in two ways. One way is step iii above, which is a rare event. The second way is *Local estimation* [10] which is used in conjunction to step vi, in every scattering event. The local estimation contributions $W_{\text{le}}$ expresses the probability that a photon scatters towards the camera and reaches the camera without interacting again. Let $\mathbf{V}_{s\to c}$ be the vector from the scattering point $\mathbf{X}_s$ to $\mathbf{X}_c$. Let $t_{s\to c}$ be the transmittance (2) along $\mathbf{V}_{s\to c}$. Let $\Phi_{\mathscr{R}_s,c}$ be the angle between $\mathscr{R}_s$ and $\mathbf{V}_{s\to c}$. Let $\varpi$, $P$ be the respective albedo and phase function of the scattering particle. If a photon scatters by an aerosol, then $\varpi = \varpi^{\text{aerosol}}$, $P = P_{\text{HG}}$. If the photon scatters by a molecule then

$\varpi = \varpi^{\text{air}}$, $P = P_{\text{Ray}}$. Local estimation then contributes

$$W_{\text{le}} = \varpi I_s P(\Phi_{\mathscr{R}_s,\text{c}}) \frac{t_{s\to c}}{|\mathbf{V}_{s\to\text{c}}|^2} \tag{13}$$

to pixel $p$ in camera $c$. The factor $|\mathbf{V}_{s\to\text{c}}|^{-2}$ can be interpreted as consideration of $\mathbf{X}_s$ to be a point radiation source. Due to this factor, FMC is unstable when the camera is *in-situ* i.e, inside the scattering medium. Local estimation from scattering points $\mathbf{X}_s$ close to $\mathbf{X}_c$ lead to a large increase of image variance. Hence, an infinite number of photons is needed for convergence when $|\mathbf{V}_{s\to\text{c}}| \to 0$.

### 1.1.3 Backward Monte Carlo Photon Tracking

Numerically, BMC is very similar to the FMC. But, there are two major difference. First, from pixel $p$ at camera $c$ a photon is launched in direction $-\boldsymbol{\omega}_p$. Then the photon is traced back through the atmosphere. A photon that happens to back-trace into the Sun, is counted as contribution to pixel $p$. The second difference is the local estimation calculation as we detail below. BMC take the following steps (Fig. 2):

(`i`) Launch a photon-packet from camera $c$ to direction $-\boldsymbol{\omega}_p$. This is the initial *ray*, denoted $\mathscr{R}_0$. The packet has an initial intensity $I_0$. Per iteration $s$:

(`ii`) Do as described in Sec. 1.1.1.

(`iii`) If $\mathbf{X}_s$ is outside the domain, the packet is terminated. If $\mathscr{R}_s || \boldsymbol{\omega}_{\text{sun}}$, the packet is counted as contributing to pixel $p$.

(`iv,v,vi`) Do as described in Sec. 1.1.1.

Here too, local estimation is preformed in conjunction to step `vi`. Here local estimation derives radiance back-traced to the sun, at each scattering event. Local estimation expresses the probability that a back propagating photon scatters towards the Sun, then reaches the Sun without interacting again. Let $\mathbf{V}_{s\to\text{sun}}$ be the vector from the scattering point $\mathbf{X}_s$ to the TOA, directed to $-\boldsymbol{\omega}_{\text{sun}}$ (Fig. 2[right]). Here $t_{s\to\text{sun}}$ is the transmittance along $\mathbf{V}_{s\to\text{sun}}$, and $\Phi_{\mathscr{R}_s,\text{sun}}$ is the angle between $\mathscr{R}_s$ and $\mathbf{V}_{s\to\text{sun}}$. Local estimation then contributes

$$W_{\text{le}} = \varpi I_s P(\Phi_{\mathscr{R}_s,\text{sun}}) t_{s\to\text{sun}}. \tag{14}$$

Since the Sun is out of the scattering medium and effectively located at infinity, there is no $|\mathbf{V}_{s\to\text{sun}}|^{-2}$ factor at all. Hence sky-images simulated by BMC are stable even in-situ. A comparison is displayed in Fig. 3: FMC rendering is very noisy compared to BMC.

# 2 A Proposed Forward Model

As described in Sec. 1, a BMC sky-image simulator has a major stability advantage over FMC. However BMC has drawbacks. BMC estimates radiance for one camera and one pixel at a time. In contrast, each single FMC sample trajectory can contribute to multiple viewpoints and pixels in parallel, using local-estimation (Fig. 2). This is efficient for simulating multiple cameras, which observe an atmospheric domain from $N_{\text{views}}$ viewpoints.

We seek to use FMC for several reasons. First, FMC is more efficient for multi-pixel multi-view simulations. Moreover, a gradient-based recovery, as in [1, 18], requires the volumetric fields $I(\mathbf{X}, \boldsymbol{\omega})$, $J(\mathbf{X}, \boldsymbol{\omega})$, not only projected images. Volumetric fields are obtained using FMC without local estimation, hence, are not prone to instabilities. To enable FMC in-situ, however, we need to overcome the $|\mathbf{V}_{s\to\text{c}}|^{-2}$ instability. In this section, we describe a solution, disposing the $|\mathbf{V}_{s\to\text{c}}|^{-2}$ factor using voxelization of the field $J$.

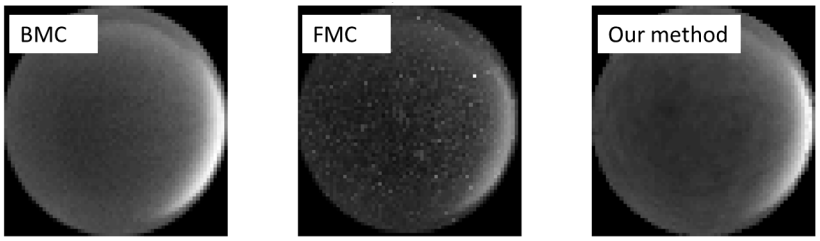


Figure 3: Comparison of rendering results using $10^7$ initial photons.

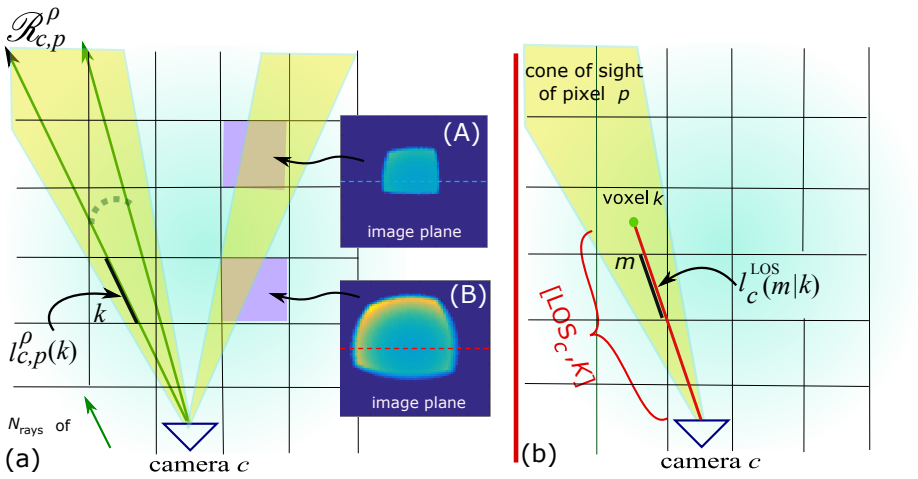


Figure 4: (a) Ray $\mathscr{R}^{\rho}_{c,p}$ intersects with voxel $k$ creating a line-segment $l^{\rho}_{c,p}(k)$. The spot size of $k$ on the image plane depends on the distance of $k$ from camera $c$ (A-B). Line-segment $l^{\text{LOS}}_{c}(m|k)$ is the intersection between voxel $m$ and line-segment $[\text{LOS}_c, k]$.

As illustrated in Fig. 1 the volumetric domain is discretized into a grid of $N_{\text{voxels}}$ rectangular cuboid voxels, indexed by $k$ or $m$. As a numerical approximation, assume that within any voxel, the parameters $\beta(k)$ ,$\sigma^{\text{aerosol}}$, $\varpi^{\text{aerosol}}$, and $g$ are constants, e.g., corresponding to the values at each voxel center.

Our RT solution has three steps: (`i`) Pre-calculate the geometry of the cameras-grid setup. (`ii`) FMC simulation calculates the radiance scattered from voxel $k$ in the direction of camera $c$. (`iii`) Light attenuation along the LOS from voxel $k$ to camera $c$.

## 2.1 Geometry

A camera sensor comprises of $N_{\text{pix}}$ pixels. Each pixel collects light from a narrow cone in the atmosphere (Fig. 4a). The cone either contains or intersects some voxels, while remaining oblivious to the rest. The radiant power contributed by voxel $k$ to camera $c$ is $R_c(k)$, which we define in detail in Sec. 2.3. Overall, radiance captured at the pixel from all voxels is a weighted sum of $R_c(k)$ over all voxels $k$. This sum is formulated by a sparse $N_{\text{pix}} \times N_{\text{voxels}}$ matrix operation $\mathbf{\Pi}_c$, having

reciprocal area units

$$\boldsymbol{i}_c = \boldsymbol{\Pi}_c \boldsymbol{R}_c \ . \tag{15}$$

Here $\boldsymbol{i}_c$ is the image, column-stacked to a vector $N_{\text{pix}}$ long, and $\boldsymbol{R}_c$ is a column-stacked representation of $R_c(k)$. The weights of $\boldsymbol{\Pi}_c$ represent the relative portion of the radiant power contributing to camera $c$, solely due to geometry.

These weights are pre-calculated as follows: Divide pixel $p$ to $N_{\text{rays}}$ points, from each of which back-project a ray $\mathscr{R}^{\rho}_{c,p}$. The intersection length of $\mathscr{R}^{\rho}_{c,p}$ (Fig. 4a) with voxel $k$ is $l^{\rho}_{c,p}(k)$. Let $V_{\text{voxel}}$ be a voxel volume. The weight is then proportional to a normalized average intersection length,

$$\boldsymbol{\Pi}_c(p,k) = \bar{l}_{c,p}(k) = \frac{1}{N_{\text{rays}} V_{\text{voxel}}} \sum_{\rho=1}^{N_{\text{rays}}} l^{\rho}_{c,p}(k) \ . \tag{16}$$

Eqs. (15,16) express rendering. There is no factor proportional to $|\mathbf{V}_{s\to \text{c}}|^{-2}$ in Eqs. (15,16). This factor is implicit in the weighted sum matrix $\boldsymbol{\Pi}_c$: each voxel contributes to several pixels, illuminating a spot in the image plane. More rays pass through voxels closer to a camera. Thus, if a scattering event occurs in a voxel for which $|\mathbf{V}_{s\to \text{c}}|$ is small, the contribution to the image affects more pixels than if the voxel had a large $|\mathbf{V}_{s\to \text{c}}|$. This is expressed by a larger spot in the image (Fig. 4a). Fig. 3 demonstrates our improvement relative to simple FMC (Sec. 1.1.1).

## 2.2 Scattered Radiance Calculation with FMC

Define the *scattered radiance* as $L(\mathbf{X}, \boldsymbol{\omega}) = J(\mathbf{X}, \boldsymbol{\omega})\beta(\mathbf{X})$. Using FMC, $L(\mathbf{X}, \boldsymbol{\omega})$ can be estimated by caching all the scattering events that occurred at $\mathbf{X}$ in direction $\boldsymbol{\omega}$. Our situation is simpler for two reasons. First, we use a voxelized radiance grid. Hence $\mathbf{X}$ is discretized to the voxel index $k$. Second, as shown below, we only need to store the scattered radiance that contributes to the discrete set of $N_{\text{views}}$ cameras $c = 1, ..., N_{\text{views}}$. We denote the power scattered from voxel $k$ in the direction of camera $c$ by $L_c(k)$. For each scattering event in voxel $k$, update $L_c(k)$ by

$$L_c(k) \leftarrow L_c(k) + \varpi I_s P(\Phi_{\mathscr{R}_s,\text{c}}). \tag{17}$$

Hence $L_c$ is discretized in space and the relevant directions. Similarly, a discrete version of $J(\mathbf{X}, \boldsymbol{\omega})$ is

$$j_c(k) = \frac{L_c(k)}{\beta(k)}. \tag{18}$$

## 2.3 Optical Transmittance

The transmittance between $\mathbf{X}$ and $\mathbf{X}_c$ is

$$t(\mathbf{X}, \mathbf{X}_c) = \exp\Big[ - \int_{\mathbf{X}_c}^{\mathbf{X}} \beta(r) dr \Big]. \tag{19}$$

Eq. (7) can be re-written as image rendering:

$$I(\mathbf{X}_c, \boldsymbol{\omega}_p) = A + \int_{\mathbf{X}_c}^{\mathbf{X}_{\partial\Omega}} L(\mathbf{X}', \boldsymbol{\omega}_p) t(\mathbf{X}', \mathbf{X}_c) d\mathbf{X}', \tag{20}$$

where $A$ represents direct solar rays entering the camera. For each camera $c$, denote by $[\text{LOS}_c, k]$ a LOS between camera $c$ and the center of voxel $k$ (Fig. 4b). Suppose this LOS intersects voxel $m$.

The geometric length of this intersecting line segment is $l_c^{\rm LOS}(m|k)$. Following Eq. (1), the optical depth between the center of voxel $k$ to camera $c$ is

$$\tau_{{\rm LOS}_c}(k) = \sum_{m\in[{\rm LOS}_c,k]} l_c^{\rm LOS}(m|k)\beta(m). \tag{21}$$

Define a $N_{\rm voxels} \times N_{\rm voxels}$ sparse matrix whose element $(k,m)$ is

$$\boldsymbol{W}_c(k,m) = \begin{cases} l_c^{\rm LOS}(m|k) & \text{if } m \in [{\rm LOS}_c, k] \\ 0 & \text{otherwise} \end{cases} . \tag{22}$$

Let $\boldsymbol{\tau}_{{\rm LOS}_c}$ and $\boldsymbol{\beta}$ be column-stack vector representations of $\tau_{{\rm LOS}_c}(k)$ and $\beta(k)$, respectively. Then, we can write Eq. (21) using matrix notation

$$\boldsymbol{\tau}_{{\rm LOS}_c} = \boldsymbol{W}_c\boldsymbol{\beta}. \tag{23}$$

The discrete transmittance from the center of voxel $k$ towards camera $c$ is

$$T_c(k) = \exp[-\tau_{{\rm LOS}_c}(k)]. \tag{24}$$

Based on Eqs. (15,17,24)

$$R_c(k) = L_c(k)T_c(k) \ . \tag{25}$$

Let $\boldsymbol{T}_c$, $\boldsymbol{L}_c$ be the column stack vector representations of ${\rm T}_c(k)$ and ${\rm L}_c(k)$ respectively. A column-stack vector of all voxel contributions to camera $c$ is described by

$$\boldsymbol{R}_c = \boldsymbol{L}_c \odot \boldsymbol{T}_c \ . \tag{26}$$

Here $\odot$ denotes the Hadamard (element-wise) product.

Let $\boldsymbol{j}_c$ be a column-stack vector representation of $j_c(k)$. Then from Eqs. (15,18,26), excluding direct sun light, the image is

$$\boldsymbol{i}_c(\boldsymbol{\beta}) = \boldsymbol{\Pi}_c(\boldsymbol{j}_c \odot \boldsymbol{Y}_c) = \boldsymbol{\Pi}_c(\boldsymbol{j}_c \odot \boldsymbol{\beta} \odot \boldsymbol{T}_c) \ \ , \tag{27}$$

where $\boldsymbol{Y}_c = \boldsymbol{\beta} \odot \boldsymbol{T}_c$. The value of pixel $p$ in image $c$ is

$$i_c(p) = \frac{1}{N_{\rm rays}V_{\rm voxel}} \sum_{\rho=1}^{N_{\rm rays}} \sum_{k\in\mathscr{R}_{c,p}^{\rho}} l_{c,p}^{\rho}(k) j_c(k)\beta(k)T_c(k). \tag{28}$$

Eqs.(15,27,28) are a discrete version of Eq. (20), excluding the direct solar irradiance of the camera.

# 3 Rendering Simulations

We tested the scenes used in [5], illustrated in Fig. 5. We briefly re-mention them here for clarity.
**Geometry**: The atmospheric domain is $50{\rm km}^2 \times 50{\rm km}^2$ wide, 10km thick. We use $80 \times 80 \times 120$ voxels of size $625 \times 625 \times 83$m. The field $\beta(\mathbf{X})$ is discretized to a coarser $20 \times 20 \times 40$ grid. The sun is at zenith angle $\Phi^{\rm SR} = 45^o$. Following [5], the sun's red-green-blue wavelengths intensity ratios are $255 : 236 : 224$. There are $N_{\rm views} = 36$ ground-based cameras placed uniformly with $\sim$ 7km nearest-neighbor separation.
**Aerosols**: Two aerosols types were used all having $\varpi^{\rm aerosol} = 1$:

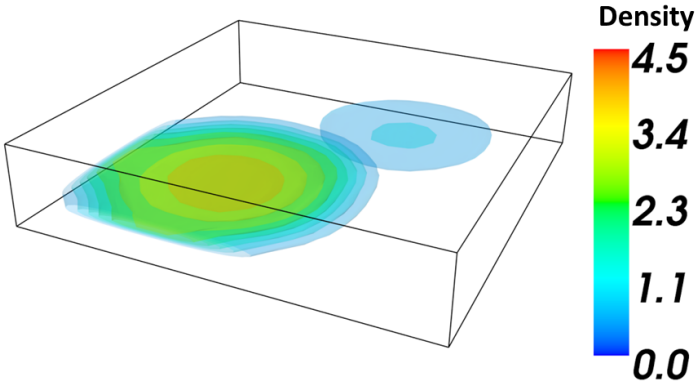


Figure 5: Aerosol distributions [5]. *Haze blobs* low density distribution. The aerosol density unit is $10^6$ particles/m$^3$.

1. An artificial aerosol having an isotropic phase function. The extinction cross sections are in the red-green-blue (RGB) channels $\sigma_{\mathrm{R}}^{\mathrm{aerosol}} = \sigma_{\mathrm{G}}^{\mathrm{aerosol}} = \sigma_{\mathrm{B}}^{\mathrm{aerosol}} = 17\ \mu\mathrm{m}^{-2}$.
2. Type 6 from the aerosol list in [7]. The anisotropy parameter per color channel is $[g_{\mathrm{R}}, g_{\mathrm{G}}, g_{\mathrm{B}}] = [0.763, 0.775, 0.786]$. The extinction cross sections are $[\sigma_{\mathrm{R}}^{\mathrm{aerosol}}, \sigma_{\mathrm{G}}^{\mathrm{aerosol}}, \sigma_{\mathrm{B}}^{\mathrm{aerosol}}] = [16.5, 16.2, 15.9]\ \mu\mathrm{m}^{-2}$.

Let $n^{\mathrm{sealevel}}$ be a density of aerosols at sea level. Here we give a short description of the atmospheres. More details are found in [5]. We simulated different aerosol distributions:

**Atm1** Haze blobs (Fig. 5) of an isotropic aerosol, at low density ($n^{\mathrm{sealevel}} \approx 10^6$).

**Atm2** Haze blobs of an anisotropic aerosol, at low density ($n^{\mathrm{sealevel}} \approx 10^6$).

**Atm3** Haze blobs of an anisotropic aerosol, at high density ($n^{\mathrm{sealevel}} \approx 10^7$).

All the $N_{\mathrm{views}}$ imaging systems have a hemispherical field with $N_{\mathrm{pix}} = 64 \times 64$. Fig. 6 compares images rendered using:

1. BMC, initial $10^4$ photons per pixel, i.e, $\approx 1.5 \cdot 10^9$ photons in total.
2. Proposed voxelized FMC, using initial $10^7$ photons on the TOA, and $N_{\mathrm{rays}} = 10$.
3. Single scattering approximation [5].

Rendering using our method is highly consistent with BMC rendering (Sec. 1.1.3), and similar to the single-scattering results [5].

**Acknowledgements:**: We are grateful to Anthony Davis, Raanan Fattal, Michael Zibulevsky for fruitful discussions. We thank Mark Sheinin, Johanan Erez, Ina Talmon, Dani Yagodin for support. YYS is a Landau Fellow - supported by the Taub Foundation. His work is conducted in the Ollendorff Minerva Center. Minerva is funded through the BMBF.

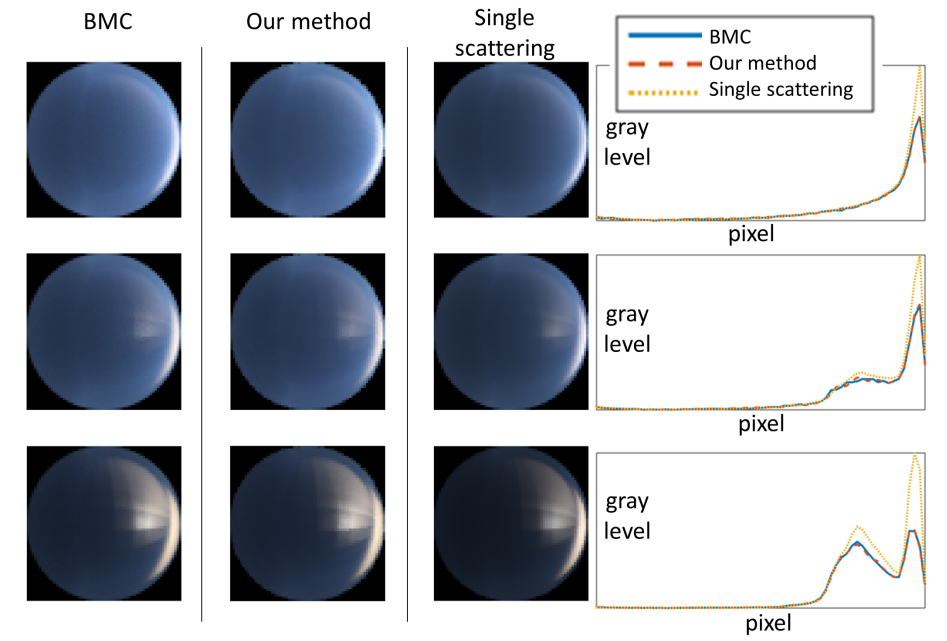


Figure 6: Image rendering and a middle horizontal line cross-section (green channel). [Top] Atm1, [middle] Atm2, and [bottom] Atm3.

# References

[1] I. Gkioulekas ,S. Zhao, K. Bala, T. Zickler, A. Levin "Inverse Volume Rendering with Material Dictionaries: Supplementary Material," ACM Transactions on Graphics (2013).

[2] S. Arridge ,J. Schotland, "Optical tomography: forward and inverse problems," arXiv preprint arXiv,0907.2586 (2009).

[3] H. Iwabuchi, "Efficient Monte Carlo Methods for Radiative Transfer Modeling," Journal of the Atmospheric Sciences **63**, 2324–2339 (2006).

[4] R. Buras ,B. Mayer "Efficient unbiased variance reduction techniques for Monte Carlo simulations of radiative transfer in cloudy atmospheres: The solution," J. Quant. Spectrosc: Radiat. Transfer **112**,434–447 (2011).

[5] A. Aides, Y. Y. Schechner, V. Holodovsky, M. Garay, A. Davis. "Multi sky-view 3D aerosol distribution recovery," Opt. Express **21**,2582025833, (2013).

[6] L. Devroye, "Sample-based non-uniform random variate generation," in *Proceedings of the 18th conference on Winter simulation,* (ACM, 1986), pp. 260–26.5

[7] J. V. Martonchik, R. A. Kahn, and D. J. Diner, "Retrieval of aerosol properties over land using MISR observations," in *Satellite Aerosol Remote Sensing over Land,* , A. A. Kokhanovsky and G. Leeuw, eds. (Springer Berlin Heidelberg, 2009), pp. 267–293.

[8] D. A. Boas, D. H. Brooks, E. L. Miller, C. A. DiMarzio, M. Kilmer, R. J. Gaudette, and Q. Zg. Imaging the body with diffuse optical tomography. *IEEE Signal Proc. Mag.*, 18(6):57–75, 2001.

[9] A. Gibson, J. Hebden, and S. R. Arridge. Recent advances in diffuse optical imaging. *Phys. Med. Biol.*, 50(4):R1, 2005.

[10] A. Marshak and A. Davis, *3D Radiative Transfer in Cloudy Atmospheres*, Physics of Earth and Space Environments (Springer, 2005).

[11] M. I. Mishchenko and I. V. Geogdzhayev, "Satellite remote sensing reveals regional tropospheric aerosol trends," Opt. Express **15**, 7423–38 (2007).

[12] J. Martonchik, D. D. J. Diner, J. M. David, R. Kahn, T. P. Ackerman, M. M. Verstraete, B. Pinty, and H. R. Gordon, "Techniques for the Retrieval of Aerosol Properties over Land and Ocean Using Multi-angle Imaging," IEEE Trans. on Geoscience and Remote Sensing **36**, 1212–1227 (1998).

[13] S. Chandrasekhar. *Radiative Transfer*. Dover Pub., 1960.

[14] J. R. Frisvad, "Importance sampling the Rayleigh phase function," Journal Of Optical Society of America **26(12)**, 2436–2441 (2011).

[15] T. Binzoni, T. S. Leung, A. H. Gandjbakhche, D. Rüfenacht, D. T. Delpy, "The use of the Henyey–Greenstein phase function in Monte Carlo simulations in biomedical optics," Physics in medicine and biology **51(17)**, N313–N322 (2006).

[16] D. Veikherman, A. Aides, Y. Y. Schechner, and A. Levis. Clouds in the cloud. *Proc. ACCV*, 2014.

[17] Y. Y. Schechner, S. K. Nayar, P. N. Belhumeur. "Multiplexing for optimal lighting," IEEE Transactions on Pattern Analysis and Machine Intelligence **29(8)**, 1339–1354 (2007).

[18] A. Levis, Y. Y. Schechner, A. Aides, A. B. Davis. "Airborne Three-Dimensional Cloud Tomography," IEEE Internetional conferens computer vision. (2015).